

# A unidimensional Monte Carlo simulation of electron drift velocities and electroluminescence in argon, krypton and xenon

Teresa H V T Dias<sup>†</sup>, A D Stauffer<sup>‡</sup> and C A N Conde<sup>†</sup>

<sup>†</sup> Departamento de Física, Universidade de Coimbra, 3000 Coimbra, Portugal

<sup>‡</sup> Department of Physics, York University, Toronto, Ontario, Canada M3J 1P3

Received 7 December 1984, in final form 17 September 1985

**Abstract.** The drift of electrons in argon, krypton and xenon is studied for the reduced electric field range of interest for electroluminescence based radiation detectors ( $E/p = 0.5$  to  $5 \text{ V cm}^{-1} \text{ Torr}^{-1}$ ), using a unidimensional Monte Carlo model which is described in detail. Appropriate factors are introduced in this model to take into account the three-dimensional nature of the electron scattering process. Electron drift velocities, reduced light output and excitation and scintillation efficiencies are obtained. Some detailed information on drift times and drift distances between elastic and inelastic collisions is also presented.

## 1. Introduction

Noble gases have played an important role in nuclear radiation detectors for a long time (Knoll 1979). Recently their range of applications has been extended to other fields such as optical radiation sources, including lasers (Rhodes 1979, Hutchinson 1980). Most of these applications concern the transport of electrons drifting in a gas under the influence of an electric field. Two main types of phenomena produced by the drifting electrons are involved, namely the induced electrical charge pulse and the electroluminescence which results from the excitation of the noble gas atoms. The first type of phenomenon is the basis for ionisation chambers, and the second one is the basis for gas scintillation and gas proportional scintillation counters (GPSC) (Conde and Policarpo 1967). The GPSC has attracted much interest due to its high energy resolution (Policarpo 1977) and large area capabilities in soft x-ray spectrometry and to its use in energy and position sensitive counters for high-energy physics and x-ray astronomy (Peacock *et al* 1980, Anderson 1981, Charpak 1982, Ku *et al* 1982, Mutterer 1982, Policarpo 1982).

Since our work was motivated by a desire to understand more fully the mechanism of the GPSC, we describe it briefly here.

When electrons produced in a noble gas by the incident ionising radiation drift under the influence of an electric field they can acquire enough kinetic energy to excite the noble gas atoms. At atmospheric pressure the excited states thus formed lead, after three-body collisions, to the formation of noble gas excimers (Suzuki and Kubota 1979, Leite 1980, Policarpo 1981). These decay within a short time—typically a few nanoseconds—emitting VUV photons in a continuum peaked at 126 nm for argon, 148 nm

for krypton and 173 nm for xenon (Suzuki and Kubota 1979). These photons (the so called secondary or proportional scintillation) are detected by a photomultiplier or a photo-ionisation chamber giving rise to an electronic pulse whose amplitude is proportional to the energy of the detected radiation.

For the heavier noble gases Ar, Kr and Xe there is a pressure reduced electric field intensity threshold close to  $E/p = 1 \text{ V cm}^{-1} \text{ Torr}^{-1}$  below which there is no electroluminescence (Feio *et al* 1982) ( $E/p = 1 \text{ V cm}^{-1} \text{ Torr}^{-1}$  is equivalent at 300 K to  $E/N = 3.11 \times 10^{-17} \text{ V cm}^2$  or 3.11 Td, where  $N$  is the number density of the gas atoms). For stronger fields the electroluminescence intensity increases in an almost linear way with the electric field strength (Conde *et al* 1977). Up to  $E/p \sim 5 \text{ V cm}^{-1} \text{ Torr}^{-1}$ , ionisation is very improbable and a single electron drifting along the field lines can produce a few hundred photons per cm before it is collected by the anode. The efficiency for conversion of electrical into optical energy is very high (besides excitation, the only other energy loss mechanism available is recoil in elastic collisions), reaching 70%–80%.

The good energy resolution achieved with detectors based on proportional scintillation is in fact due to the large amount of light produced and to the fact that there are no statistical fluctuations introduced in the number of electrons through ionisation, as GPSC operate in the  $E/N$  range where the probability for electron multiplication is zero or very low.

It is essential to understand quantitatively the phenomena involved in the transport of electrons in noble gases (electroluminescence, diffusion parameters, etc) to further their applications in the field of radiation detectors and optical sources. For this purpose two main techniques are commonly used: Boltzmann analysis (Frost and Phelps 1964, Lowke and Parker 1969, Huxley and Crompton 1974, Pitchford and Phelps 1981, 1982, Crompton 1983, Ogawa 1984) and Monte Carlo simulation (Itoh and Musha 1960, Thomas and Thomas 1969, McIntosh 1974, Lucas and Saele 1975, Milloy and Watts 1977, Braglia 1977, Sakai *et al* 1977, Küküparci and Lucas 1981, Boeuf and Marode 1982, Davies *et al* 1984).

Computer experiments using Monte Carlo methods, as described in this work, although very demanding in computing time, provide a direct method of testing the physical mechanisms assumed, by comparing the simulation results with data obtained from real experiments. On the other hand, Monte Carlo simulation may provide information not available from Boltzmann analysis or from a real experiment, thus enlarging the scope of understanding of the processes under study. Boltzmann equation analysis is difficult to carry out when spatially non-uniform distributions and non-equilibrium processes are involved. For instance, there is evidence that low-current discharges in very pure noble gases display luminous layers (Holst and Oosterhuis 1921, Druyvesteyn 1931, Hayashi 1982, Fletcher 1985) which imply spatially non-uniform distributions. This is also the case for the electroluminescence phenomena we study in this work, where the Monte Carlo method allows us to obtain a detailed description of the spatially-dependent processes involved, as we show in table 1 and illustrate in figure 11.

In this work, we use a unidimensional Monte Carlo simulation to study the electron drift velocities and electroluminescence in noble gases, in the  $E/N$  range of interest for GPSC work.

Some preliminary results on electroluminescence in xenon have already been published using this model (Dias *et al* 1983).

In order to use the Monte Carlo method a knowledge of the relevant cross sections is required. These are discussed in § 2. In § 3 we describe the details of our Monte Carlo simulation and present the results in § 4.

**Table 1.** Results for (a) argon, (b) krypton and (c) xenon ( $p = 760$  Torr,  $T = 300$  K).

$E/p$ (V cm <sup>-1</sup> Torr <sup>-1</sup> )	$E/N$ (Td)	Averages between two successive collisions		Averages between two successive inelastic collisions		
		Drift distance (nm)	Drift time (ps)	Number of elastic colls ( $\times 10^3$ )	Drift distance ( $\mu\text{m}$ )	Drift time (ns)
<b>(a) Argon</b>						
0.50	1.55	677	0.95	—	—	—
1.00	3.11	471	0.59	—	—	—
1.50	4.66	389	0.46	$232.2 \pm 216.3$	$412 \pm 284$	$107.4 \pm 102.9$
2.00	6.21	364	0.43	$78.0 \pm 70.7$	$158 \pm 73$	$33.0 \pm 32.3$
2.50	7.77	349	0.41	$41.0 \pm 35.7$	$97 \pm 31$	$16.6 \pm 15.6$
3.00	9.32	337	0.39	$24.9 \pm 21.2$	$70 \pm 16$	$9.7 \pm 9.2$
3.50	10.87	327	0.38	$17.0 \pm 13.6$	$55 \pm 10$	$6.4 \pm 5.7$
4.00	12.43	321	0.37	$13.3 \pm 11.2$	$46 \pm 8$	$5.0 \pm 4.7$
4.50	13.98	316	0.37	$10.9 \pm 9.2$	$40 \pm 6$	$4.0 \pm 3.8$
5.00	15.53	309	0.36	$8.5 \pm 7.0$	$35 \pm 5$	$3.1 \pm 2.8$
<b>(b) Krypton</b>						
0.75	2.33	340	0.47	—	—	—
1.00	3.11	310	0.39	$897.0 \pm 533.0$	$799 \pm 380$	$351.8 \pm 221.1$
1.50	4.66	268	0.34	$156.0 \pm 131.7$	$172 \pm 69$	$51.7 \pm 45.8$
2.00	6.21	259	0.33	$72.8 \pm 59.4$	$97 \pm 25$	$23.1 \pm 20.4$
2.50	7.77	252	0.31	$41.5 \pm 34.4$	$67 \pm 13$	$12.8 \pm 11.5$
3.00	9.32	250	0.30	$27.3 \pm 22.7$	$52 \pm 8$	$8.3 \pm 7.6$
3.50	10.87	244	0.30	$19.6 \pm 16.5$	$43 \pm 6$	$5.7 \pm 5.4$
4.00	12.43	243	0.29	$15.7 \pm 12.9$	$37 \pm 6$	$4.6 \pm 4.3$
4.50	13.98	238	0.28	$12.7 \pm 10.5$	$33 \pm 5$	$3.6 \pm 3.2$
5.00	15.53	238	0.28	$10.2 \pm 8.2$	$29 \pm 4$	$2.9 \pm 2.7$
<b>(c) Xenon</b>						
0.50	1.55	238	0.39	—	—	—
0.75	2.33	195	0.31	—	—	—
1.00	3.11	174	0.26	$881.1 \pm 611.0$	$426 \pm 214$	$231.5 \pm 181.5$
1.50	4.66	161	0.23	$241.5 \pm 172.3$	$136 \pm 44$	$53.4 \pm 42.9$
2.00	6.21	160	0.23	$113.8 \pm 88.6$	$78 \pm 17$	$25.4 \pm 22.2$
2.50	7.77	153	0.21	$65.3 \pm 53.8$	$55 \pm 10$	$13.3 \pm 12.4$
3.00	9.32	152	0.21	$45.2 \pm 37.9$	$44 \pm 7$	$9.4 \pm 8.6$
3.50	10.87	150	0.20	$34.6 \pm 29.3$	$36 \pm 6$	$7.1 \pm 6.6$
4.00	12.43	148	0.20	$25.9 \pm 20.9$	$31 \pm 5$	$5.1 \pm 4.6$
4.50	13.98	147	0.20	$21.0 \pm 15.6$	$27 \pm 4$	$3.6 \pm 3.4$
5.00	15.53	148	0.20	$16.8 \pm 12.9$	$24 \pm 4$	$3.3 \pm 2.9$

## 2. Electron scattering cross sections

Reliable scattering cross sections, both elastic and inelastic, are an essential requirement for any particle transport Monte Carlo simulation. In this section we summarise the data which were used throughout our calculations for argon, krypton and xenon.

### 2.1. Elastic scattering

The elastic differential  $\sigma_e(\theta)$  and integral  $\sigma(\epsilon)$  cross sections were obtained from theor-

etical phase shifts  $\delta_l(0 \leq l \leq 50)$  using the well known expressions

$$\sigma_\varepsilon(\theta) = k^{-2} \left| \sum_l \exp(i\delta_l) \sin \delta_l (2l + 1) P_l(\cos \theta) \right|^2 \quad (1)$$

$$\sigma(\varepsilon) = (4\pi/k^2) \sum_l (2l + 1) \sin^2 \delta_l \quad (2)$$

where  $k$  is the electron wavenumber corresponding to energy  $\varepsilon$  ( $\varepsilon = 13.6025 k^2$ , with  $\varepsilon$  in eV and  $k$  in au).

As the  $E/N$  range of interest for the present work is a low and restricted one, the  $l = 0$  to  $l = 6$  polarised orbital model phase shifts from McEachran and Stauffer (1983) for argon and from McEachran and Stauffer (1984) for krypton were chosen, as both sets of data are reliable especially at low energies. In the case of xenon, however, the  $l = 0$  to  $l = 6$  phase shifts were taken from Sin Fai Lam (1982), as relativistic effects, which become important for this gas, were taken into account in that author's calculations. Analytical fittings to the  $l = 0$  to  $l = 6$  phase shifts were accomplished in every case, to facilitate the calculation of the scattering cross sections at any energy using equations (1) and (2) (for xenon the appropriate relativistic formulae were used instead of (1) and (2) (Mott and Massey 1965, p 228)).

From  $l = 7$  to  $l = 50$  we use the effective range formulae of Ali and Fraser (1977) for the phase shifts.

A full discussion of the mentioned phase shifts and resulting cross sections together with a complete comparison with earlier data can be found in the sources we mention, i.e. in McEachran and Stauffer (1983, 1984) and Sin Fai Lam (1982).

## 2.2. Inelastic scattering

At the low  $E/N$  values with which we worked, only the lowest excited levels are expected to be reached for most of the events when excitation occurs. Thus the corresponding excitation cross sections are the most relevant and we have treated them individually as far as possible.

At present there is very little information on the electron impact excitation cross sections for the individual electronic excitation levels of argon, krypton and xenon. Where published values are available, only a few points can be found across the electron energy range we are interested in, i.e. from threshold to about 15–20 eV.

For the first four excited states of argon and krypton (1s5, 1s4, 1s3 and 1s2 in the Paschen notation) we did simple polynomial fits to the experimental partial excitation cross section data previously published for Ar (Chutjian and Cartwright 1981) and Kr (Trajmar *et al* 1981), extrapolating down to the thresholds. For xenon, where similar data are not available in the literature, educated guesses were made below 15 eV assuming linear variation with energy and relative magnitudes similar to those published for krypton (Trajmar *et al* 1981).

To take into account the excitation of the remaining levels, a fifth excited pseudo-state was then considered. Its threshold (14.0 eV for Ar, 12.5 eV for Kr and 10.8 eV for Xe) was taken by averaging over the structure of the excitation functions obtained from Brion and Olsen (1970) and Cvejanovic and Read (1974). The excitation cross section of this pseudo-level was taken as a smoothly increasing function from its threshold which, together with the previously mentioned four levels, would join the total excitation cross sections of de Heer *et al* (1979), whose data meets the end of our range of interest (15–20 eV). As an example, figure 1 shows the inelastic cross sections for  $e^-$  in Ar used in

this work. If we add the five excited states inelastic contributions described above, the resulting total excitation cross sections tend to be situated lower than the total excitation data of Schaper and Scheibner (1969) for Ar, Kr and Xe, and also lower than those more recently recommended by Ferreira and Loureiro (1983) for Ar, and by Hayashi (1983) for Xe. However, we verified that increasing our particular choices of partial excitation

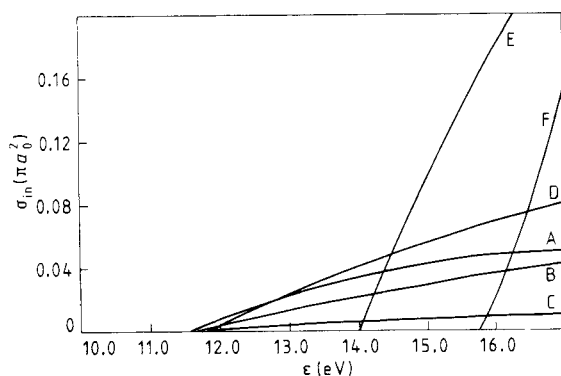


**Figure 1.** Inelastic scattering cross sections for electrons on Ar (ps refers to pseudo-state, see § 2.2). Curves: A, 1s5; B, 1s4; C, 1s3; D, 1s2; E, ps; F, ion.

cross sections by a factor of 2 did not affect significantly the results obtained in this work, as we shall see later.

The ionisation cross sections we used were also simple polynomial fits to the well established data from Rapp and Englander-Golden (1965).

### 2.3. Total scattering cross section

Having adopted the integral elastic, partial excitation and ionisation cross sections described in the previous sections, and to be consistent with our choice, we simply added the respective contributions to obtain  $\sigma_t(\epsilon)$  in the energy range we worked—up to a few eV above inelastic threshold. The variation in the published results for both the total and the integral elastic cross sections is such that a more precise determination would be impossible at present (cf McEachran and Stauffer, 1983, 1984).

For each of the noble gases argon, krypton and xenon, the total (elastic + excitation + ionisation) scattering cross section  $\sigma_t(\epsilon)$  was then fitted by  $\sim 20$  cubic splines, accomplishing a better than 1% agreement with the values we calculated.

The fittings to all phase shifts and cross sections will be published in detail in a forthcoming paper (Stauffer *et al* 1986) in a way suitable for low-energy electron transport Monte Carlo simulation work.

## 3. The unidimensional Monte Carlo simulation

For readers not familiar with the general features of a standard particle transport Monte Carlo simulation, we refer them to Cashwell and Everett (1959), Carter and Cashwell (1975), Duderstadt and Martin (1979) and James (1980).

While the processes involved in the drifting of electrons are actually three-dimensional, the unidimensional model we developed (§§ 3.1 and 3.2) achieves a good agree-

ment with experimental data. In spite of the fact that it is a unidimensional model, it contains the essential processes.

(i) The electron anisotropic scattering is taken into account through an energy dependent backward/forward scattering probability.

(ii) The electron energy loss through recoil in elastic collisions with the noble gas atoms is also considered using an energy dependent backward/forward momentum transfer factor.

(iii) The variation of the total scattering cross section due to the electron acceleration along each individual free path is also taken into consideration.

The details will be given in §§ 3.1 and 3.2. Throughout these sections we use the following notation.

$E$	electric field strength
$e, m$	electron charge and mass
$M$	the gas atom mass
$N$	number density of the gas atoms
$\gamma$	$= m/M$
$\mu$	$= mM/(m + M)$ , the reduced mass of the electron-gas atom system
$v_g$	velocity of the gas atom in the laboratory frame
$\lambda, \tau$	length and duration of one free path of the electron
$v_0, v_1, v$	initial, final and instantaneous velocities of the electron in the laboratory frame when one free path is considered
$v_r$	$= v - v_g$ , the instantaneous velocity relative to the gas atom (centre of mass frame)
$\epsilon$	$= \frac{1}{2}\mu v_r^2$ , the instantaneous energy in the centre of mass frame.

All velocities have algebraic values.

### 3.1. The free path

The electron is assumed to move only along linear paths parallel to the uniform electric field direction, colliding at the end of each free walk with a gas molecule whose velocity  $v_g$  is a random number from the gaussian Maxwell velocity component distribution at the considered temperature (300 K).

The length  $\lambda$  of an individual free path in any Monte Carlo electron drift simulation is determined by a second random number  $R$  which is related to the path integral by

$$\ln R = -N \int_0^\lambda \sigma_r d\lambda \quad (3)$$

or

$$\ln R = -N \int_{v_0}^{v_1} \sigma_r v dt \quad (4)$$

where  $\sigma_r$  is the total scattering cross section and  $R$  is uniformly distributed in the interval [0–1].

Assuming that the electron motion is unidimensional, i.e. that the electron is bound to move only along the field lines, its laboratory and relative velocities are

given by

$$v = v_0 + eE/m t$$

$$v_r = v_0 + eE/m t - v_g$$

at any instant  $t$  along the path.

The path integral (4) then becomes

$$\ln R = -(Nm/eE) \int_{v_{r0}}^{v_{r1}} \sigma_t(\varepsilon) (v_r + v_g) dv_r. \quad (5)$$

As  $v_g$  is of the order of  $10^{-4}v_r$  in the range of  $E/N$  we use, and the uncertainty in  $\sigma_t$  is certainly larger than that factor, it is reasonable to approximate the integral by

$$\begin{aligned} \ln R &= -(Nm/eE) \int_{v_{r0}}^{v_{r1}} \sigma_t(\varepsilon) v_r dv_r \\ &= -(Nm/\mu eE) \int_{\varepsilon_0}^{\varepsilon_1} \sigma_t(\varepsilon) d\varepsilon. \end{aligned} \quad (6)$$

As the total cross section  $\sigma_t(\varepsilon)$  was fitted by cubic splines, the solution  $\varepsilon_1$  of the integral equation (6) is the root of a fourth-degree polynomial in  $\varepsilon$ . The *regula falsi* successive approximation method was used to find the root  $\varepsilon_1$  for each path (the more efficient Newton–Raphson method failed to converge near  $\varepsilon = 0$ ).

We should emphasise that the magnitude of the random number determines the ‘shape’ of each particular free electron trajectory in the sense that electrons which start with  $v_0 < 0$ , i.e. against the accelerating field, may or may not turn around during one free random walk according to the  $R$  value.

Once  $\varepsilon_1$  is found,  $v_{r1}$  and  $v_1$  are obtained from

$$v_{r1} = \pm (2\varepsilon_1/\mu)^{1/2} \quad (7)$$

where the sign was determined by the sign of  $v_0$  and by the magnitude of  $R$ , and

$$v_1 = v_{r1} + v_g. \quad (8)$$

The position  $z$  of the electron relative to the previous collision and the time interval  $\tau$  between collisions are then computed by

$$z = (\frac{1}{2}mv_1^2 - \frac{1}{2}mv_0^2)/eE \quad (9)$$

$$\tau = (v_1 - v_0)/(eE/m). \quad (10)$$

After a number of collisions, the final position  $Z$  and elapsed time  $T$  will be  $Z = \Sigma z$  and  $T = \Sigma \tau$ .

### 3.2. The collision process

At the end of each free path the electron will suffer a collision whose kind—elastic, excitation to 1s5, 1s4, 1s3, 1s2 or pseudo-state or ionisation—will be decided upon through the use of a third random number. If  $\varepsilon_1$  is the energy at which the collision occurs, the sum of the cross sections for the allowed processes at that energy is normalised to 1 and divided into intervals proportional to each individual cross section: the random number falls into one of those intervals and in this way determines which kind of collision occurs.

Two main groups of electron collisions may be considered: elastic and inelastic.

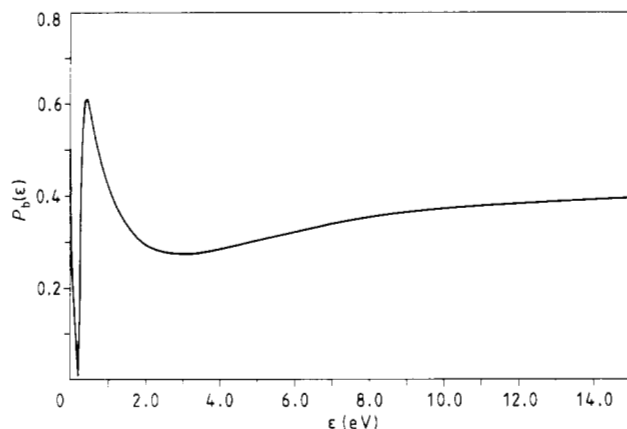


Figure 2. Probability of backward elastic scattering for electrons on argon.

3.2.1. *Elastic collisions.* This type of collision is by far the most important in our case, since most of the collisions that occur are elastic for the  $E/N$  range we considered. Special care was taken in making their treatment as accurate as possible.

As our model is a unidimensional one, the first decision to make when a collision occurs is whether the electron is going to be scattered forward or backward. In order to take this decision correctly, we construct the following backward scattering probability function  $P_b(\epsilon)$ :

$$P_b(\epsilon) = \frac{\int_{\pi/2}^{\pi} \sigma_\epsilon(\theta) \sin \theta d\theta}{\int_0^{\pi} \sigma_\epsilon(\theta) \sin \theta d\theta} \quad (11)$$

by averaging the elastic differential cross section  $\sigma_\epsilon(\theta)$  over the backward hemisphere.

Values of  $P_b(\epsilon)$  were tabulated at 0.05 eV intervals,  $\sigma_\epsilon(\theta)$  being integrated numerically. If  $\epsilon_1$  is the energy at which the collision occurs,  $P_b(\epsilon_1)$  is obtained by linear interpolation between the two nearest tabulated values, and the forward/backward decision is made by comparing a fourth random number with the magnitude of  $P_b(\epsilon_1)$  (the forward probability is of course the complement of 1).

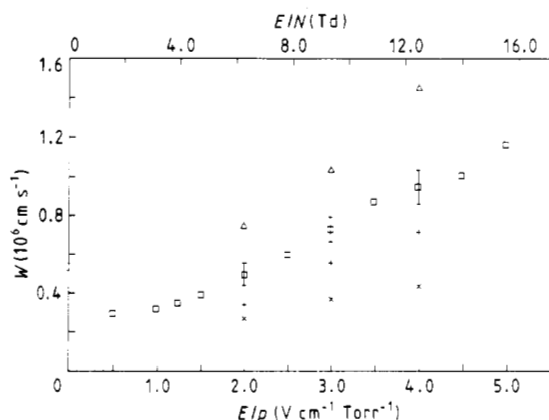


Figure 3. Electron drift velocity in argon calculated with:  $P_b = 0.25$  ( $\Delta$ );  $P_b = 0.50$  (+);  $P_b = 0.75$  ( $\times$ );  $P_b(\epsilon)$  as in figure 1 and equation 11 ( $\square$ ).

The backward scattering probability function  $P_b(\epsilon)$  is plotted in figure 2 for argon as an example.  $P_b(\epsilon)$  for krypton and xenon show similar structure although the features are a little less pronounced as we go from argon to krypton to xenon. This plot shows clearly how anisotropic the scattering really is: even at very small energies  $P_b(\epsilon)$  shows drastic and rapidly varying deviations from the initial isotropic 0.5 value, and although  $P_b(\epsilon)$  shows less structure at higher energies, its magnitude is always well under 0.5 here.

We wish to emphasise that  $P_b(\epsilon)$  represents the probability of scattering in the direction opposite to the motion of the electron before the collision and not necessarily in the direction opposite to the accelerating field. Further we have verified for instance that for the case of xenon at  $E/p = 3.0 \text{ V cm}^{-1} \text{ Torr}^{-1}$ , in less than 1% of the free paths did the electrons go through energy zero. This is in part due to the fact that the elastic cross section increases very rapidly as the energy of the electron approaches zero. This behaviour is true for all the heavier noble gases (cf McEachran and Stauffer 1983, 1984) and this means that a change in direction of the electron due to the electric field itself is very unlikely, i.e. there is a low probability of the electron having zero velocity. Almost all changes in direction of the electron are due to collisions with gas atoms.

To show how sensitive the results can be to the changes in  $P_b(\epsilon)$ , we plot in figure 3 the argon drift velocities computed with the correct  $P_b(\epsilon)$  (from equation (11) and shown in figure 2) together with the drift velocities obtained using the constant values  $P_b = 0.25, 0.50, 0.75$  while keeping the same  $\sigma_e(\epsilon)$ . The deviations from the correct values are substantial even in the case of  $P_b = 0.50$  which corresponds to isotropic scattering. Similar though less pronounced deviations were observed in the calculated electroluminescence yield.

The next step is to calculate the electron energy loss in the elastic collision itself, thus obtaining the initial conditions for the next free path.

In a real three-dimensional process the energy lost in an elastic collision would be given by

$$\Delta\epsilon = \epsilon' - \epsilon_1 = -\frac{2\gamma}{(\gamma + 1)^2} (1 - \cos \theta) \epsilon_1 \tag{12}$$

where  $\theta$  is the scattering angle and  $\epsilon'$  is the energy after the collision.

In our unidimensional model, to calculate the momentum transferred to the gas atom in an elastic collision we introduce two energy-dependent momentum transfer factors— $TM_f(\epsilon)$  for forward scattering and  $TM_b(\epsilon)$  for backward scattering—by averaging over the corresponding hemisphere:

$$TM_f(\epsilon) = \int_0^{\pi/2} (1 - \cos \theta) \sigma_\epsilon(\theta) \sin \theta \, d\theta \bigg/ \int_0^{\pi/2} \sigma_\epsilon(\theta) \sin \theta \, d\theta \tag{13}$$

$$TM_b(\epsilon) = \int_{\pi/2}^{\pi} (1 - \cos \theta) \sigma_\epsilon(\theta) \sin \theta \, d\theta \bigg/ \int_{\pi/2}^{\pi} \sigma_\epsilon(\theta) \sin \theta \, d\theta. \tag{14}$$

$\Delta\epsilon$  is then approximated by

$$\Delta\epsilon = \begin{cases} -2\gamma/(\gamma + 1)^2 TM_f(\epsilon_1) \epsilon_1 & \text{forward scattering} \\ -2\gamma/(\gamma + 1)^2 TM_b(\epsilon_1) \epsilon_1 & \text{backward scattering.} \end{cases} \tag{15}$$

$$\tag{16}$$

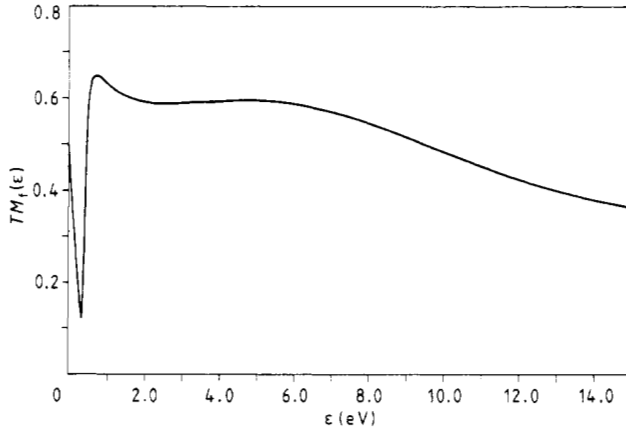


**Figure 4.** Forward momentum transfer factor for electrons on argon.

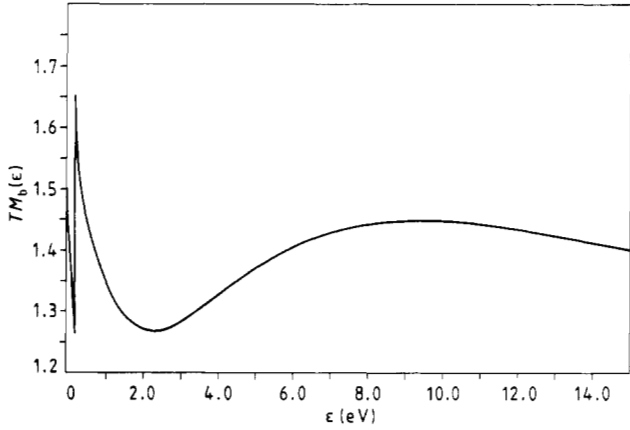


**Figure 5.** Backward momentum transfer factor for electrons on argon.

After the collision we have then

$$\varepsilon' = \varepsilon_1 + \Delta\varepsilon \tag{17}$$

$$v_r'^2 = v_{r1}^2 + 2\Delta\varepsilon/\mu = v_{r1}^2 - 2\gamma/(\gamma + 1)^2 v_{r1}^2 TM_{f,b} \tag{18}$$

and

$$v_r' = w v_{r1} [1 - 2\gamma/(\gamma + 1)^2 TM_{f,b}]^{1/2} \tag{19}$$

where  $w = +1$  for forward scattering and  $w = -1$  for backward scattering.

Finally the electron velocity in the laboratory frame after the collision, the new  $v_0$ , is

$$v_0 = v_r' + v_g. \tag{20}$$

At this point a new  $v_g$  is sampled and we repeat the whole procedure beginning in § 3.1.

The  $TM_f$  and  $TM_b$  values were tabulated at 0.05 eV intervals, and the  $TM$  value

at the current energy was then obtained by interpolating between the two appropriate values. Figure 4 and figure 5 show plots of  $TM_f(\epsilon)$  and  $TM_b(\epsilon)$  using argon as an example. Plots for krypton and xenon behave similarly.

**3.2.2. Inelastic collisions.** When the collision happens to be inelastic, the energy loss is assumed to be equal to the energy of the corresponding level in the case of excitation or to the ionisation potential in the case of ionisation. When ionisation occurs, one half of the electron excess energy is taken as the new energy for each of the two resulting electrons, which are assumed to have the same history from then on (this approximate way of treating the two resulting electrons is a simplification which does not affect the results, as in the energy range of the present calculations only a few ionisation events actually occur).

#### 4. Results

Figures 6–8, 10, 11 and tables 1, 2 show the results of our simulation experiments when a group of  $\sim 30$  electrons, with initial velocities sampled from a gaussian Maxwell velocity component distribution, was allowed to drift along a fixed

**Table 2.** Total excitation  $Q_{\text{exc}}$  and scintillation  $Q_{\text{sc}}$  efficiencies.

$E/p$ (V cm <sup>-1</sup> Torr <sup>-1</sup> )	$E/N$ (Td)	$Q_{\text{sc}}$ (%)			$Q_{\text{sc}}$ (%)		
		Ar	Kr	Xe	Ar	Kr	Xe
0.50	1.55	0.0	0.0	0.0	0.0	0.0	0.0
0.75	2.33	0.0	1.3	2.6	0.0	1.1	2.2
1.00	3.11	3.3	15.7	27.4	2.8	13.1	23.2
1.50	4.66	25.4	51.9	55.0	21.5	43.3	46.9
2.00	6.21	49.1	68.7	71.4	41.4	57.1	60.4
2.50	7.77	63.7	79.0	80.2	53.5	65.5	67.8
3.00	9.32	73.8	85.0	85.4	61.8	70.2	71.9
3.50	10.87	80.2	88.3	88.5	66.8	72.8	74.3
4.00	12.43	83.4	90.3	89.6	69.3	74.2	74.6
4.50	13.98	85.8	91.4	90.4	71.2	75.0	75.3
5.00	15.53	87.9	92.4	92.1	72.5	75.7	76.6

distance, 3.5 mm for Ar, 2.5 mm for Kr and 1.5 mm for Xe, so that the number of collisions turns out to be of the same order of magnitude in each case. The quantities of interest are obtained by averaging over the whole group of electrons. The simulations were carried out at  $T = 300$  K and  $p = 760$  Torr in the  $E/p$  range relevant to GPSC work, typically  $\sim 0.5$  to  $5.0$  V cm<sup>-1</sup> Torr<sup>-1</sup> (corresponding to  $E/N \sim 1.6$  to  $15.5$  Td). The noble gas collision velocities are sampled from a gaussian Maxwell velocity component distribution.

Drift velocities were calculated by averaging the  $Z/T$  values over the whole group of electrons. These Monte Carlo results are plotted in figures 6, 7 and 8 for argon, krypton and xenon, respectively, as a function of the reduced electric field. They show a good agreement with experimental values found in the literature (Dutton 1975, Bowe 1960, Pack and Phelps 1961, Pack *et al* 1962, Christophorou *et al* 1979, Cumpstey and Vass 1980, Brooks *et al* 1982) which are also shown for comparison.

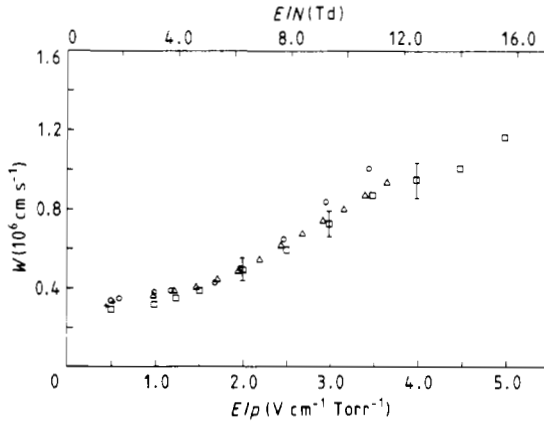


**Figure 6.** Electron drift velocity in argon:  $\square$ , our calculation;  $\triangle$ , Bowe (1965); +, Pack *et al* (1961);  $\circ$ , Christophorou *et al* (1979).

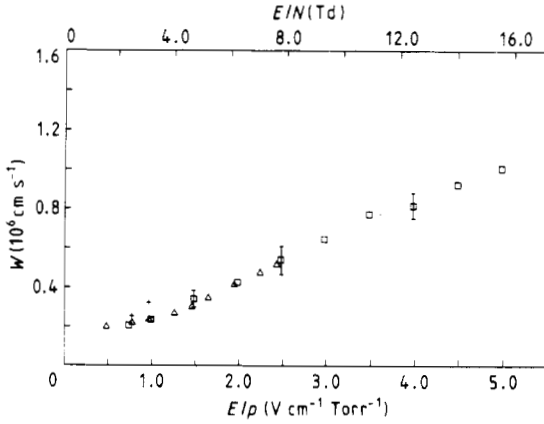


**Figure 7.** Electron drift velocity in krypton:  $\square$ , our calculation;  $\triangle$ , Bowe (1965); +, Pack *et al* (1962).

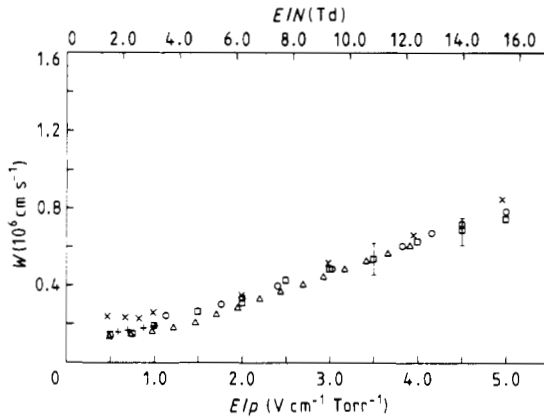


**Figure 8.** Electron drift velocity in xenon:  $\square$ , our calculation;  $\triangle$ , Bowe (1965);  $\times$ , Brooks *et al* (1982);  $\circ$ , Cumpstey and Vass (1980); +, Pack *et al* (1962).

As we have already mentioned, the drift velocity results show an important sensitivity to the extent of the anisotropy introduced in the calculations (while keeping the same  $\sigma_i(\epsilon)$ ), as was shown in figure 3.

The  $E/N$  range we use in the present simulation experiments does not allow for electron avalanches (several thousand elastic collisions occur between any two successive inelastic collisions, see table 1), the inelastic scattering being only a very small fraction of the total scattering. So our results on drift velocities are not sensitive to the unavoidable uncertainty in the excitation cross sections, as this uncertainty will not affect the total cross section in any appreciable way (as an example, a non-significant change in the drift velocity, i.e. smaller than the statistical spread of the calculations shown in figure 8, was observed for xenon at  $E/p = 4.5 \text{ V cm}^{-1} \text{ Torr}^{-1}$  when all five partial excitation cross sections were increased by a factor of 2 in the simulation).

We should state that in the case of xenon, the only case where relativistic cross sections were used, the agreement of our drift velocity results with experimental data was improved by the use of these elastic cross sections. The xenon non-relativistic data we used in Dias *et al* (1983) tended to produce overestimated drift velocities.

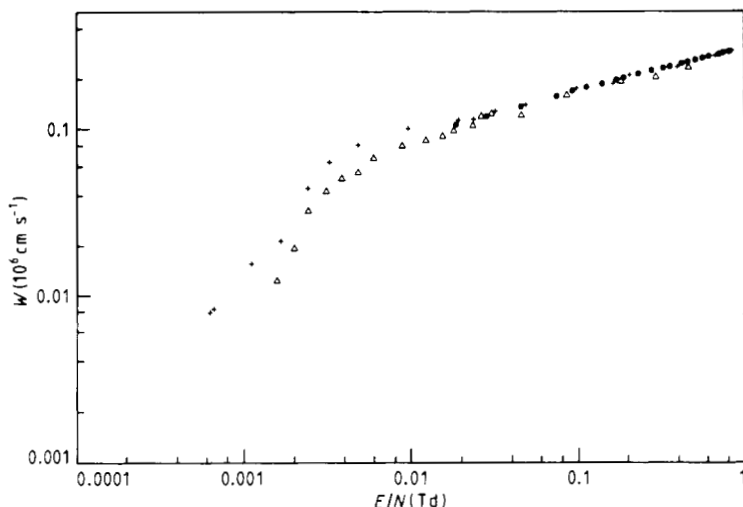


**Figure 9.** Electron drift velocity in argon for  $E/N < 1 \text{ Td}$ .  $\Delta$ , our calculation; +, Pack and Phelps (1961);  $\bullet$ , Robertson (1977).

We have also extended our calculations for argon to very low values of  $E/N$  ( $< 1 \text{ Td}$ ) to be able to compare electron drift velocities with existing experimental data in this region (Pack and Phelps 1961, Robertson 1977). The results are shown in figure 9. In this particular case they were obtained by the simulation of the drift of one electron through 6.5 cm (the 3.5 mm drift distance in Ar used in our calculations at higher  $E/N$ —see beginning of this section—proved to be insufficient to stabilise the calculated results in most of this low  $E/N$  range). A good agreement with experiment is also found in this region, where the electron energies are in the vicinity of the Ramsauer minimum and the scattering cross section is rapidly varying.

In the present simulation experiments we have also studied the electroluminescence produced while electrons drift along the field, in the  $E/N$  range of interest for proportional scintillation work.

Every time an excitation occurs in a collision, we assume that a photon with the energy characteristic of the peak of the excited dimer continuum VUV emission (9.8 eV for  $\text{Ar}_2^*$ , 8.4 eV for  $\text{Kr}_2^*$  and 7.2 eV for  $\text{Xe}_2^*$ ) is emitted. Considering the whole group of electrons, we computed the reduced light output—the number of photons produced by one electron per unit distance per unit pressure—as a function of the reduced electric field (Conde *et al* 1977). The results thus obtained for argon, krypton and xenon are plotted in figure 10.

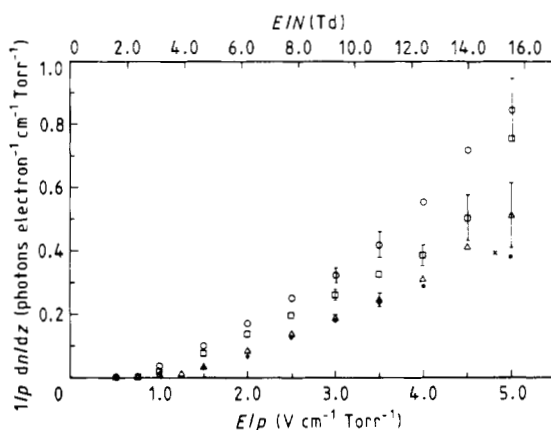


**Figure 10.** Argon ( $\Delta$ ), krypton ( $\square$ ) and xenon ( $\circ$ ) reduced light output as computed in this work. Excitation coefficients for argon:  $\bullet$ , Lagushenko and Maya (1984);  $\times$ , Ferreira and Loureiro (1983).

So far, absolute experimental values for this quantity have not been measured with good precision. Although our light output results are expected to be affected by the uncertainty on the excitation cross sections, the influence is still negligible at the low  $E/N$  we used, as most of the collisions are elastic and an electron within a range of energies which allow for excitation will spend a long time and suffer a great number of collisions before excitation successfully occurs (at  $E/p = 4.5 \text{ V cm}^{-1} \text{ Torr}^{-1}$  in xenon, a non-significant difference, i.e. within the statistical spread of the calculations shown in figure 10, was observed in the computed light output when all the five partial excitation cross sections were increased by a factor of 2).

Theoretical and experimental values of the threshold for light production have been published (Feio *et al* 1982 and references therein). Although they are scattered over a wide range in the vicinity of  $E/p = 1 \text{ V cm}^{-1} \text{ Torr}^{-1}$ , they are consistent with our results. The computed threshold for light production is completely determined by the extent of momentum transfer in elastic collisions compared to what is gained from the field along free paths.

Above this threshold, our calculated reduced light output increases linearly with  $E/p$  until the ionisation threshold is reached: this is also the behaviour shown by the experimental data (Conde *et al* 1977, Andresen *et al* 1977, Cumpstey and Vass 1980, Leite *et al* 1981, 1982, Policarpo 1982).

Since in our calculations we assume that one photon is produced for every excitation event, our reduced light output results can also be compared with some excitation coefficients available in the literature calculated through Boltzmann analysis. Those which fall within our range (Ar) are included in figure 10 and agree very well with our

results. Above  $E/p = 4.5 \text{ V cm}^{-1} \text{ Torr}^{-1}$  in Ar, the production of extra electrons by ionisation, which is starting to occur, introduces larger fluctuations and leads to a steeper increase in the number of excitations (i.e. photons) obtained in our calculation: once ionisation is present, the reduced light output we calculate will depend on the drift distance considered, as the number of electrons will increase with that distance. This would account for the apparent discrepancy at  $E/p \sim 5.0 \text{ V cm}^{-1} \text{ Torr}^{-1}$  in figure 10 between our reduced light output and the excitation coefficients there reported.

There has been recently a renewed interest in the study of the distribution of luminous layers displayed in low-pressure discharges in noble gases before an equilibrium is reached (Hayashi 1982, Fletcher 1985). At the range of  $E/N$  we scan in the present study (which while being a low one already allows for excitation and consequent photon production), this spatial periodicity of the photon emission is also expected. This is evidenced by the existence of a characteristic value, for each  $E/N$  value, of the average distance travelled by one electron between successive inelastic collisions as shown in table 1. The distributions of these distances have a rather small variation about the mean value, which explains the appearance of discrete luminous layers under the appropriate conditions. Thus for argon with  $E/p = 3.0 \text{ V cm}^{-1} \text{ Torr}^{-1}$  we would expect, at  $p = 760 \text{ Torr}$ ,  $T = 300 \text{ K}$ , to have the first layer centred at  $70 \mu\text{m}$  from the source of electrons, the second layer somewhat broader centred at  $140 \mu\text{m}$ , etc. Our range of  $E/N$  is still low enough to exclude or minimise the possibility of ionisation which, when producing a significant number of extra electrons, tends to blur the separation between the layers by introducing large fluctuations in the number of photons produced.

On the other hand, table 1 also shows that the distributions of drift times and number of elastic collisions between two successive inelastic collisions always have variations of the order of the mean values. The variation in the drift times accounts for the experimental difficulty in resolving in time the producing of photons and shows that position sensitive techniques using gas proportional scintillation counters should be based on drifting distances rather than on drifting times. The very high number of elastic collisions that occur on average before an electron succeeds in exciting an atom (table 1) and the very small energy gained between two elastic collisions (77 meV, 57 meV, 35 meV for Ar, Kr, Xe, respectively, at  $E/p = 3.0 \text{ V cm}^{-1} \text{ Torr}^{-1}$ , see table 1) explain how crucial it is to use extremely pure noble gases in GPSC work: the presence of even a small percentage of an impurity has a very good chance of quenching the process of noble gas atom excitation and consequent photon emission.

We call the attention of the reader to the fact that for a fixed value of  $E/p$  the drift times and drift distances listed in table 1(a,b,c) are inversely proportional to the pressure  $p$ , so that for each  $E/p$  ( $E/N$ ) those results refer only to the conditions stated in the tables ( $p = 760 \text{ Torr}$ ,  $T = 300 \text{ K}$ ), but they can be transformed easily if different conditions are considered.

In figure 11 (simulation in xenon,  $E/p = 3.0 \text{ V cm}^{-1} \text{ Torr}^{-1}$ ) the evolution of the energy and position (plotted every 100 collisions) of a particular electron along the field can be followed, showing in detail the process of energy gain from the field and energy loss in elastic collisions through momentum transfer to the atoms, together with the ultimate high losses caused by the inelastic collisions. Most of the collisions occur at energies above the Ramsauer minimum, the presence of this minimum in the scattering cross section being clearly evidenced in figure 11 by the energy gap in the beginning of each plotted cycle.

Note that figure 11 is just depicting a detail taken from our xenon calculations, which were extended over 1.5 mm for each one of a group of  $\sim 30 \text{ e}^-$  (see beginning of this

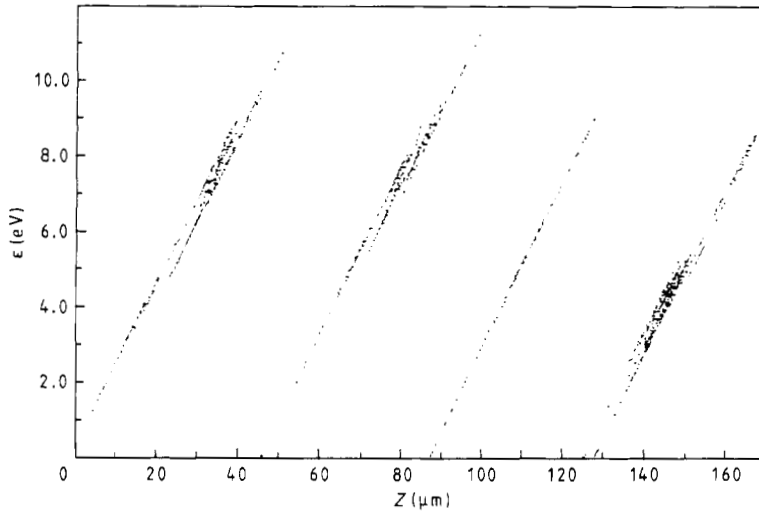


Figure 11. Energy versus position of one electron, plotted every 100 collisions ( $E/p = 3.0 \text{ V cm}^{-1} \text{ Torr}^{-1}$ ,  $e^-$  in xenon)

section) producing the results shown in figures 8 and 10 and tables 1(c) and 2 for electrons in xenon at  $E/p = 3.0 \text{ V cm}^{-1} \text{ Torr}^{-1}$ .

In the range of  $E/N$  we studied, the energy gained by the electrons from the electric field can be converted into optical energy with very high efficiency, as the energy lost by the electron in elastic collisions is very small and yet ionisation events are still very few. In table 2 we show the results obtained for the total excitation and scintillation efficiencies for argon, krypton and xenon. These two quantities are defined as the fraction of the electron energy gained from the electric field which is used for excitation and which is carried by the VUV photons, respectively. The total excitation efficiency was computed by adding the partial excitation efficiencies corresponding to the five states considered (see § 2.2). The total scintillation efficiency was obtained considering that the available optical energy is the product of the total number of excitations to the same five states multiplied by the energy of the photon emitted by the excited dimer (every excitation is assumed to result in the production of a photon, as stated before). Excitation efficiency in GPSC has been treated in Feio *et al* (1980) where an experimental value of 97% (with a margin of 20%) for krypton is quoted (note that the quantity which is named scintillation efficiency by those authors is actually an excitation efficiency).

The data in table 2 show that VUV radiation sources can in principle be built with an optimised efficiency of conversion of electrical into optical energy if a reduced electric field of  $4.5\text{--}5.0 \text{ V cm}^{-1} \text{ Torr}^{-1}$  is used. Above this range, ionisation lowers that efficiency.

Although the ratio  $Q_{sc}/Q_{exc}$  is not constant in principle, the data in table 2 show that  $Q_{sc}/Q_{exc} = 0.83 \pm 0.01$  in agreement with the fact that, within the range of our calculations, the first four excited states are those predominantly excited.

## 5. Conclusions

The unidimensional Monte Carlo method which we have developed in this paper gives good results for the drift velocities and electroluminescence of noble gases in the low

$E/N$  range, allowing us to predict as well other electron transport quantities as given in tables 1 and 2.

In this unidimensional model the general Monte Carlo particle transport path integral equation.

$$\ln R = -N \int_{v_0}^{v_1} \sigma_t v dt$$

is reduced to

$$\ln R = -(Nm/\mu eE) \int_{\epsilon_0}^{\epsilon_1} \sigma_t(\epsilon) d\epsilon.$$

Great care was taken to introduce in this unidimensional approximation the appropriate factors which take into account the three-dimensional nature of the electron collision processes. A much more elaborate treatment is necessary for a full three-dimensional simulation, unless some simplifying assumptions are introduced for momentum transfer and angular scattering during the collisions (e.g. isotropic scattering). This unidimensional approach can be seen as a successful compromise between accuracy and computational effort when a correct treatment is required. Below the threshold for light production, the energy which the electrons acquire from the electric field is entirely lost through momentum transfer in elastic collisions so that excitation of atoms and the consequent production of photons never occur while electrons drift along a sufficiently low reduced electric field. We can see that momentum transfer plays an important role not only in the determination of the photon emission threshold but also in the way excitation and scintillation efficiencies grow with  $E/N$  before a maximum is reached.

An easy and detailed use of elastic and inelastic data throughout the simulations was possible by the introduction of analytical fittings to all required cross sections as functions of energy.

The agreement of our results with previous experimental work shows that mechanisms based on the direct excitation of the noble gas atoms by the electrons can fully account for the secondary light production. There is no need to consider other processes like collisions with ground state dimers or neutral bremsstrahlung.

The use of a unidimensional approach was a first attempt to obtain absolute and direct results on electroluminescence yields and excitation and scintillation efficiencies in the range of  $E/N$  of interest for GPSC. More definite data on electron impact partial excitation cross sections in noble gases near threshold would help to improve the results on the electroluminescence in GPSC presented here, although these were shown not to be strongly affected by the uncertainty in that data.

The authors are developing an experimental procedure to measure, at low pressure and within the  $E/N$  range of this present study, the spatial distribution of the luminous layers displayed by noble gases, in order to confirm the computed results of separation between layers and scintillation efficiencies as a function of  $E/N$  (tables 1 and 2).

We also intend to repeat these calculations using a full three-dimensional treatment and taking into account angular variation in scattering and momentum transfer. More sophisticated techniques, such as the null collision method (Skullerud 1968, Lin and Bardsley 1978) will be used to reduce the amount of calculation required. A comparison with our present results will enable us to make a more definitive evaluation of the unidimensional model developed here.

## Acknowledgments

We acknowledge support from INIC (Lisboa) and NATO (Research Grant 133/80). We thank Professor L Alte da Veiga and Professor Margarida R Costa for the use of the PDP-11/34 computer donated by the Deutsche Gesellschaft für Technische Zusammenarbeit. We also thank Professor M Salette Leite for some valuable discussions.

## References

- Ali M A and Fraser P A 1977 *J. Phys. B: At. Mol. Phys.* **10** 3091–104  
 Anderson D F 1981 *Proc. INS Symp. on Nuclear Radiation Detectors, March 23–26, INS University of Tokyo*  
 Andresen R D, Leiman E A and Peacock 1977 *Nucl. Instrum. Meth.* **140** 371–4  
 Boeuf J P and Marode E 1982 *J. Phys. D: Appl. Phys.* **15** 2169–87  
 Bowe J C 1960 *Phys. Rev.* **117** 1411–15  
 Braglia G 1977 *Physica C* **92** 91–112  
 Brion C E and Olsen L A R 1970 *J. Phys. B: At. Mol. Phys.* **3** 1020–32  
 Brooks H L, Cornell M C, Fletcher J, Littlewood I M and Nygaard K J 1982 *J. Phys. D: Appl. Phys.* **15** L51–3  
 Carter L L and Cashwell E D 1975 *USERDA Critical Review Series TID-26607*  
 Cashwell E D and Everett C J 1959 *A Practical Manual on the Monte Carlo Method for Random Walk Problems* (New York: Pergamon)  
 Charpak G 1982 *Nucl. Instrum. Meth.* **196** 1–9  
 Christophorou L G, McCorkle D L, Maxey D V and Carter J G 1979 *Nucl. Instrum. Meth.* **163** 141–9  
 Chutjian A and Cartwright D C 1981 *Phys. Rev. A* **23** 2178–93  
 Conde C A N and Policarpo A J P L 1967 *Nucl. Instrum. Meth.* **53** 7–12  
 Conde C A N, Requiça Ferreira L and Ferreira M F A 1977 *IEEE Trans. Nucl. Sci.* **NS-24** 221–4  
 Crompton R W 1983 *Proc. XVth Int. Conf. Phenomena in Ionised Gases, Dusseldorf* (Dusseldorf: Henkel KGa. A.)  
 Cumpstey D E and Vass D G 1980 *Nucl. Instrum. Meth.* **171** 473–8  
 Cvejanovic S and Read F H 1974 *J. Phys. B: At. Mol. Phys.* **7** 1180–93  
 Davies A J, Dutton J, Evans C J, Goodings A and Stewart P K 1984 *J. Phys. D: Appl. Phys.* **17** 287–99  
 Dias T H V T, Stauffer A D and Conde C A N 1983 *IEEE Trans. Nucl. Sci.* **NS-30** 389–93  
 Druyvesteyn M J 1932 *Z. Phys.* **73** 33–44  
 Duderstadt J J and Martin W R 1979 *Transport Theory* (New York: Wiley) ch. 9  
 Dutton J 1975 *J. Phys. Chem. Ref. Data* **4**  
 Feio M A, Policarpo A J P L and Alves M A F 1982 *Japan. J. Appl. Phys.* **21** 1184–90  
 Feio M A, Policarpo A J P L, Charpak G and Sauli F 1980 *Nucl. Instrum. Meth.* **176** 473–6  
 Ferreira C M and Loureiro J 1983 *J. Phys. D: Appl. Phys.* **16** 1611–21  
 Fletcher J 1985 *J. Phys. D: Appl. Phys.* **18** 221–8  
 Frost L S and Phelps A V 1964 *Phys. Rev. A* **136** 1538–44  
 Hayashi M 1982 *J. Phys. D: Appl. Phys.* **15** 1411–8  
 ——— 1983 *J. Phys. D: Appl. Phys.* **16** 581–9  
 de Heer F J, Jansen R H and van der Kaay W J 1979 *J. Phys. B: At. Mol. Phys.* **12** 979–1002  
 Holst G and Oosterhuis E 1921 *Physica* **1** 78–87  
 Hutchinson M H R 1980 *Appl. Phys.* **21** 95–144  
 Huxley L G H and Crompton R W 1974 *The Diffusion and Drift of Electrons in Gases* (New York: Wiley)  
 Itoh T and Musha T 1960 *J. Phys. Soc. Japan* **15** 1675–80  
 James F 1980 *Rep. Prog. Phys.* **43** 1145–89  
 Knoll G F 1979 *Radiation Detection and Measurement* (New York: Wiley)  
 Ku W H-M, Hailey C J and Vartanian M H 1982 *Nucl. Instrum. Meth.* **196** 63–7  
 Küçükarpacı H N and Lucas J 1981 *J. Phys. D: Appl. Phys.* **14** 2001–14  
 Lagushenko R and Maya J 1984 *J. Appl. Phys.* **55** 3293–9  
 Leite M S P 1980 *Port. Phys.* **11** 53–100  
 Leite M S P, Alves M A F, Policarpo A J P L and Feio M A 1982 *Nucl. Instrum. Meth.* **198** 587–92  
 Leite M S P, Policarpo A J P L, Feio M A and Alves M A F 1981 *Nucl. Instrum. Meth.* **179** 295–300

- Lin S L and Bardsley J N 1978 *Comp. Phys. Commun.* **15** 161–3
- Lowke J J and Parker J H 1969 *Phys. Rev.* **181** 290–311
- Lucas J and Saele H T 1975 *J. Phys. D: Appl. Phys.* **8** 640–50
- McEachran R P and Stauffer A D 1983 *J. Phys. B: At. Mol. Phys.* **16** 4023–38
- 1984 *J. Phys. B: At. Mol. Phys.* **17** 2507–18
- McIntosh A I 1974 *Aust. J. Phys.* **27** 59–71
- Milloy H B and Watts O 1977 *Aust. J. Phys.* **30** 73–82
- Mott N F and Massey H W 1965 *The Theory of Atomic Collisions* 3rd edn (Oxford: Clarendon) p 228
- Mutterer M 1982 *Nucl. Instrum. Meth.* **196** 73–81
- OGawa I 1984 in *Swarms of Ions and Electrons in Gases* ed. W Lindinger, T D Mark, F Howorka (Vienna: Springer) pp. 265–83
- Pack J L and Phelps A V 1961 *Phys. Rev.* **121** 798–806
- Pack J L, Voshall R E and Phelps A V 1962 *Phys. Rev.* **127** 2084–89
- Peacock A, Andresen R D, Leimann E A, Long A E, Manzo G and Taylor B G 1980 *Nucl. Instrum. Meth.* **169** 613–25
- Pitchford L and Phelps A V 1981 *Phys. Rev. A* **23** 294–304
- 1982 *Phys. Rev. A* **25** 540–54
- Policarpo A J P L 1977 *Space Sci. Instrum.* **3** 77–107
- 1981 *Phys. Scr.* **23** 539–49
- 1982 *Nucl. Instrum. Meth.* **196** 53–62
- Rapp D and Englander-Golden P 1965 *J. Chem. Phys.* **43** 1464–79
- Rhodes Ch K (ed.) 1979 *Topics Appl. Phys.* vol 30, *Excimer Lasers* (Berlin: Springer)
- Robertson A G 1977 *Aust. J. Phys.* **30** 39–49
- Sakai Y, Tagashira H and Sakamoto S 1977 *J. Phys. D: Appl. Phys.* **10** 1035–49
- Schaper M and Scheibner H 1969 *Beitr. Plasmaphys.* **9** 45–58
- Sin Fai Lam L T 1982 *J. Phys. B: At. Mol. Phys.* **15** 119–42
- Skullerud H R 1968 *J. Phys. D: Appl. Phys.* **1** 1567–8
- Stauffer A D, Dias T H V T and Conde C A N 1985 *Nucl. Instrum. Meth. A* **242** 327–37
- Suzuki M and Kubota 1979 *Nucl. Instrum. Meth.* **164** 197–9
- Thomas R W L and Thomas W R L 1969 *J. Phys. B: At. Mol. Phys.* **2** 562–70
- Trajmar K R, Srivastava S K, Tanaka H, Nishimura H and Cartwright D C 1981 *Phys. Rev. A* **23** 2167–77